J. Fluid Mech. (1982), *vol.* 114, *pp.* 59–82
Printed in Great Britain

The two- and three-dimensional instabilities of a spatially periodic shear layer

By R. T. PIERREHUMBERT† AND S. E. WIDNALL

Department of Aeronautics and Astronautics,
Massachusetts Institute of Technology, Cambridge, MA 02139

(Received 23 April 1980 and in revised form 16 March 1981)

The two- and three-dimensional stability properties of the family of coherent shear-layer vortices discovered by Stuart are investigated. The stability problem is formulated as a non-separable eigenvalue problem in two independent variables, and solved numerically using spectral methods. It is found that there are two main classes of instabilities. The first class is subharmonic, and corresponds to pairing or localized pairing of vortex tubes; the pairing instability is most unstable in the two-dimensional limit, in which the perturbation has no spanwise variations. The second class repeats in the streamwise direction with the same periodicity as the basic flow. This mode is most unstable for spanwise wavelengths approximately $\frac{2}{3}$ of the space between vortex centres, and can lead to the generation of streamwise vorticity and coherent ridges of upwelling. Comparison is made between the calculated instabilities and the observed pairing, helical pairing, and streak transitions. The theoretical and experimental results are found to be in reasonable agreement.

1. Introduction

Experimental evidence that has been accumulating over the past few years has led to a profound advance in the understanding of the structure of turbulence in the free shear layer. Numerous observers have documented the formation and persistence of highly organized two-dimensional vortices in the course of development of a shear layer downstream of a splitter plate (see, for example, Winant & Browand 1974; Brown & Roshko 1974; Roshko 1976; Browand & Weidman 1976; Koochesfahani *et al.* 1979). The vortices have been observed under a widely varying set of flow conditions, and Wygnanski *et al.* (1979) have demonstrated the remarkable resistance of the structures to interfering influences. It is clear that any further theory of shear-layer development will have to take into account the dynamics of interaction of these large vortices. Vortex pairing, a two-dimensional interaction whereby neighbouring vortices amalgamate to form a larger vortex, has been experimentally implicated in shear-layer growth (Winant & Browand 1974). Other experiments have shown that the two-dimensional structures are subject to three-dimensional instabilities (Miksad 1972; Breidenthal 1978; Bernal *et al.* 1979; Browand & Troutt 1980). The three-dimensional instabilities are involved in the generation of small-scale erratic flow

† Present address: Department of Meteorology, Massachusetts Institute of Technology, Cambridge, MA 02139.

(Miksad 1972; Bernal *et al.* 1979) but do not destroy the large-scale coherent structures (Browand & Troutt 1980). The vortex interactions thus play a role in the important stage of transition to three-dimensionality, and, indeed continue to influence the characteristics of the developed turbulence downstream. Yet there have been few successful theoretical attempts to account for the wealth of phenomena uncovered. In the present work, we shall attempt to account for a number of the observed features of shear-layer development in terms of the instability of a row of large vortices to certain two and three-dimensional perturbations. To facilitate this study, we will introduce a number of simplifications. Firstly, we will deal only with shear flow in a homogeneous, incompressible fluid, as experiments on this simple case have revealed many features in common with the more complicated case of the mixing layer between fluids of different density. Secondly, we will assume inviscid dynamics throughout; this assumption will always be valid sufficiently far downstream of the splitter plate where scales become large, as the free shear layer does not suffer the influence of boundaries. Finally, we will deal with the temporal development of a shear layer created at an initial instant of time rather than the spatial development of a shear layer originating at a splitter plate. The temporal problem is far more tractable than the analogous spatial problem. In the case where the velocity difference between the two streams is small compared to the average velocity, the Taylor hypothesis (or Galilean transformation) can be used to relate rigorously the spatial problem to the temporal problem, as the shear layer then varies very little on a scale comparable to the vortex size. We will assume that predictions based on the Taylor hypothesis are at least qualitatively correct even when the transformation is not strictly valid. It will be seen that the quantitative match between predicted and observed growth rates is quite good even when the velocity difference is an appreciable fraction of the average velocity.

In the present work, we will investigate the linear stability of a periodic row of vortices arranged as in figure 1. The key difference between the present work and previous work on the subject resides in the choice of base state used to model the streamwise inhomogeneities of the shear layer. Earlier theoretical attempts to account for the observed instabilities have relied on one of the two limits in which the stability problem becomes analytically tractable: the very large vortex limit in which the shear layer deviates only slightly from a parallel shear layer, or the small vortex limit in which the vortices are so concentrated that they may be regarded as point vortices.

The work of Kelly (1967) on two-dimensional disturbances and of Benney & Lin (1960) on three-dimensional disturbances, belong to the near-parallel case. Kelly considered the stability of a base state consisting of the sum of a hyperbolic tangent velocity profile and the spatial part of the most unstable eigenmode of that profile. This choice was made on the basis of a Landau expansion of the equilibrated final state arising from the initial Helmholtz instability, truncated after the second term on the grounds that a highly truncated expansion is sufficient when the final state is nearly parallel. Indeed, the observed r.m.s. fluctuating velocity is generally only 10–20 % of the velocity difference ΔU; however, this is not a good measure of the validity of the near-parallel assumption, as not just the velocity, nor even the vorticity, but the vorticity *gradients* appear in the stability equations. The gradients of vorticity can be very large even when the fluctuating velocities are quite small. The results of this effect are vividly apparent in figure 2, where we have compared the

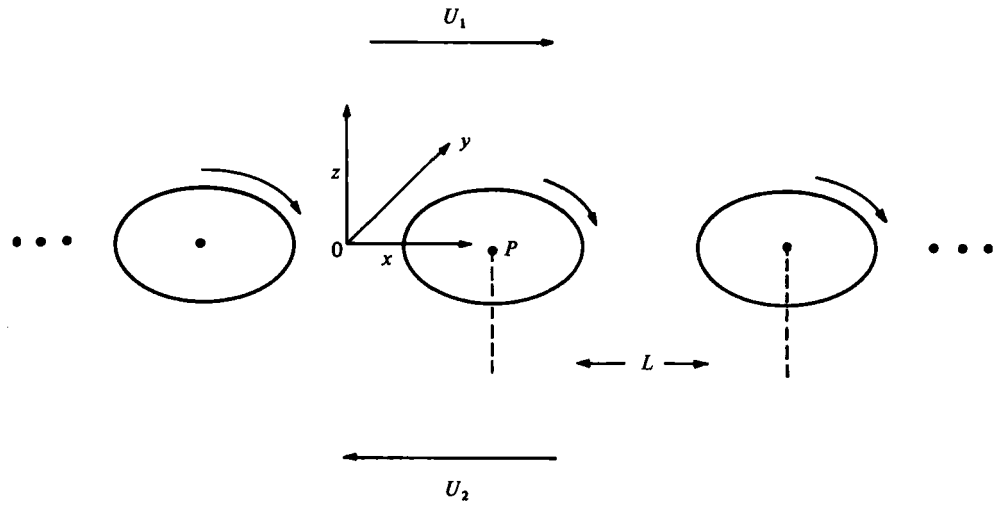

FIGURE 1. Definition of co-ordinate system for the free shear layer. The curves each represent a typical vorticity contour. The vortices repeat indefinitely to the left and right.

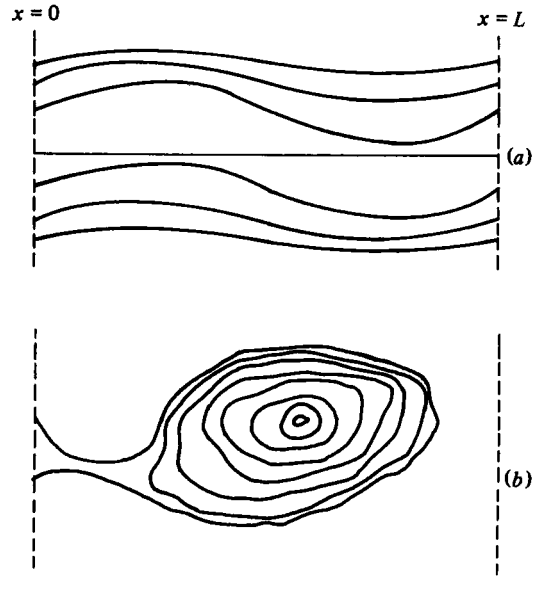

FIGURE 2. Final state vorticity patterns: (*a*) Two-term Landau expansion in near-parallel regime. (*b*) Observed vorticity distribution (after Browand & Weidman 1976, figure 6*a*).

vorticity contours of a two-term Landau expansion with the vorticity contours observed by Browand & Weidman. The observed flow in figure 2(*b*) takes the form of a nearly symmetric, flattened vortex, with mostly closed contour lines, whereas the two-term Landau expansion corresponds to a wavy shear layer. The observed vortex can be accurately modelled as a steady-state solution of the Euler equations in two dimensions, without resorting to a Landau expansion. Browand & Weidman compared the vortex with the family of steady states discovered by Stuart (1967), with stream functions given by

$$\Psi = \tfrac{1}{2}\ln[\cosh 2z - \rho\cos 2x], \tag{1}$$

where ρ is a constant between 0 and 1, which parametrizes the family. In this formula and all subsequent ones, we adopt the convention that the vortex spacing $L = \pi$ and the velocity jump $\Delta U = 2$. The best overall fit is obtained with $\rho = 0{\cdot}25$, in which case the vorticity contours agree well over the central portion of the vortex, although the observed vorticity decays somewhat more rapidly than that of the Stuart vortex towards the edge of the region containing vorticity. From equation (1), the x mean and the fluctuating parts of the z gradient of vorticity can be easily computed, and we have found that, for $\rho = 0{\cdot}25$, the maximum fluctuating part is fully 76 % of the mean part at $z = 0{\cdot}3$, and 110 % of the mean part at $z = 0{\cdot}1$. We see, then, that the observed vortices are well into the non-parallel regime. The near-parallel theory fails to represent correctly the observed equilibrated vortex structure, and neglects terms in the stability equation which in the observed situation are not negligible. The Benney–Lin mechanism is not formulated in terms of a stability problem, but nevertheless relies on the interaction of weakly nonlinear waves in a parallel shear flow and, like the Kelly theory, cannot be applied to the observed deeply non-parallel regime as typified by figure 2(*b*).

While it is clear that the observed vortices are not so large as to lead to near-parallel flow, it is equally clear that they are not so small as to be pointlike. This is evident in figure 2(*b*), and also in the results of the various flow-visualization studies that have been performed on the free shear layer. This observation is in agreement with our earlier theoretical work on uniform vortices (Pierrehumbert & Widnall 1981), which showed that energetic constraints require any vortex row produced by roll-up of a thin shear layer to have a vortex width of at least 50 % of the vortex spacing. The instability of a row of co-rotating point vortices discussed by Lamb (1932) has a number of features in common with the pairing interaction, but, in light of the fact that the observed vortices are not pointlike, it is difficult to make confident predictions based on Lamb's calculation. In the three-dimensional case, it is tempting to apply the results of Bliss (1973), Tsai & Widnall (1976) and Moore & Saffman (1975*b*) relating to vortex-tube instabilities, to the vortex tubes present in the observed shear layer. However, these theoretical results are valid at the observed spanwise wavenumber of instability only when the vortex cross-sections are nearly circular, a situation that obtains only when the vortices are pointlike.

To avoid the inadequacies inherent in the aforementioned simplified models, we will represent the equilibrated state of the shear layer with a suitably chosen steady solution to the Euler equations in two dimensions. Specifying that the solution be periodic in x and asymptotic to uniform streams for $z = \pm\infty$ guarantees a flow geometrically similar to that shown in figure 1, but does not uniquely specify the flow; indeed, equation (1) defines a continuous family of such solutions, and other families have been identified (Pierrehumbert & Widnall 1981). Presumably, the realized vorticity distribution is determined by viscous smoothing of the periodically rolled-up vortex sheet that evolves from the initial Helmholtz instability. In any event, we have seen that the Stuart vortices fit the observed distribution reasonably well; we will discuss the stability properties of only the Stuart vortices in detail, although the solution method to be described below is equally applicable to an arbitrary steady state. The stability calculation is conceptually simple, but leads to a partial-differential equation eigenvalue problem in two independent variables (x and z) which must be solved numerically. With contemporary fast computers and efficient algorithms

(notably spectral differentiation and the LR algorithm), this problem can be solved quite economically. The stability equations represent an extension of the Rayleigh problem to the strongly non-parallel case and reveal some novel stability characteristics not present when the steady flow streamlines are circular or parallel.

2. Mathematical formulation of the stability problem

We take a co-ordinate system with x pointing in the streamwise direction, y in the spanwise direction, and z chosen to complete a right-hand co-ordinate system, as depicted in figure 1. The origin of the co-ordinate system is taken midway between two vortex centres. We require that the flow be asymptotic to a uniform x velocity U_1 for $z \to +\infty$, and to U_2 for $z \to -\infty$; further, without loss of generality, we set $U_2 = -U_1$ and take units such that $U_1 = 1$. In practice, this boundary condition will be implemented by assuming that the deviation from a free stream is essentially a decaying potential flow for a sufficiently large distance d above or below the shear layer. The evolution of the flow is governed by the x and y vorticity equations

$$-\partial_t \omega_x = \mathbf{V}.\nabla\omega_x - \boldsymbol{\omega}.\nabla V_x, \quad -\partial_t \omega_y = \mathbf{V}.\nabla\omega_y - \boldsymbol{\omega}.\nabla V_y, \tag{2a, b}$$

together with the divergence relation

$$\partial_z \omega_z = -\partial_x \omega_x - \partial_y \omega_y, \tag{2c}$$

and the equations linking velocity to vorticity

$$\nabla^2 \boldsymbol{\Psi} = -\boldsymbol{\omega}, \quad \mathbf{V} = \nabla \times \boldsymbol{\Psi}. \tag{2d, e}$$

We will investigate the evolution of small perturbations to a steady solution to equation (2) which is periodic in x and a function of x and z alone. To this end, we posit the existence of a steady solution with vorticity $\boldsymbol{\omega}_0 = \hat{\mathbf{y}}\,\Omega(x, z)$ with associated velocity fields $W_x(x, z)$ and $W_z(x, z)$. Under these assumptions, the steady solution is determined by $\mathbf{W}.\nabla\Omega = 0$, which is satisfied whenever the stream function Ψ is an arbitrary function of Ω. Equation (1) describes such a solution, with vortex spacing $L = \pi$. Denoting perturbations to the steady flow quantities by $\mathbf{V}'$, $\boldsymbol{\omega}'$, and $\boldsymbol{\Psi}'$, we seek modal solutions of the form

$$\begin{pmatrix} \mathbf{V}' \\ \boldsymbol{\omega}' \\ \boldsymbol{\Psi}' \end{pmatrix} [x, y, z, t] = \begin{pmatrix} \tilde{\mathbf{V}} \\ \tilde{\boldsymbol{\omega}} \\ \tilde{\boldsymbol{\Psi}} \end{pmatrix} [x, z]\, e^{i(\alpha x + \beta y)}\, e^{-\sigma t} \tag{3}$$

where quantities with a tilde are periodic in x with period L. No constraints are placed on α and β, save that they be real. As we will be dealing only with linearized equations for the disturbances, the choice of exponential dependence in y and t is justified by the fact that the base state Ω is independent of y and t. Similarly, the assumed form of x dependence is a consequence of the periodicity of the base state. The question of the completeness of the set of all solutions of this form is an extremely difficult one, which we will make no attempt to answer in the present work.

It is now a straightforward matter to linearize (2) around the steady state, using the functional dependences indicated in (3). This procedure results in the linear system

$$\mathbf{W}.\nabla_h \tilde{\omega}_x - \tilde{\boldsymbol{\omega}}.\nabla_h W_x + i\alpha W_x\, \tilde{\omega}_x - i\beta\Omega \tilde{V}_x = \sigma\tilde{\omega}_x, \tag{4a}$$

$$\mathbf{W}.\nabla_h \tilde{\omega}_y - \tilde{\mathbf{V}}.\nabla_h \Omega + i\alpha W_x\, \tilde{\omega}_y - i\beta\Omega \tilde{V}_y = \sigma\tilde{\omega}_y, \tag{4b}$$

$$\partial_z \tilde{\omega}_z = -(i\alpha + \partial_x)\tilde{\omega}_x - i\beta\tilde{\omega}_y, \tag{4c}$$

$$[(i\alpha + \partial_x)^2 - \beta^2 + \partial_{zz}]\tilde{\Psi} = -\tilde{\omega}, \tag{4d}$$

$$\tilde{\mathbf{V}} = (\hat{\mathbf{x}}(i\alpha + \partial_x) + i\beta\hat{\mathbf{y}} + \hat{\mathbf{z}}\partial_z) \times \tilde{\Psi}, \tag{4e}$$

where $\nabla_h = \hat{\mathbf{x}}\partial_x + \hat{\mathbf{z}}\partial_z$. In subsequent discussion, the tildes will be omitted. The x boundary conditions are that all perturbation quantities in (4) be periodic in x with period L, which is consistent because of the periodicity of the coefficients of the system. The z boundary conditions are that the perturbation flow quantities match to a decaying potential flow at $z = \pm d$. This requires that the perturbation vorticity vanish at $z = \pm d$. It also imposes a boundary condition on Ψ which is most conveniently stated in terms of the Fourier decomposition of Ψ. If $\Psi(m, z)$ is the coefficient of $e^{i(2\pi m/L)x}$, this boundary condition is

$$\partial_z \Psi(m, z)|_{z=\pm d} = \mp \gamma_m \Psi(m, \pm d), \tag{5}$$

where $\gamma_m = ((\alpha + (2\pi m/L))^2 + \beta^2)^{\frac{1}{2}}$. Except in the case $m = \alpha = \beta = 0$, the boundary conditions determine Ψ uniquely via (4d). In the stated exceptional case, the undetermined part of the stream function is just a constant, which does not affect the velocity when $\alpha = \beta = 0$. Thus, given a vorticity field satisfying the boundary conditions, the associated perturbation velocity field is uniquely determined. In fact, only the x and y vorticity need be specified, since the z vorticity can be directly computed directly from (4c). Note, however, that the requirement of vanishing z vorticity at $z = d$ places a constraint on the z-average part of the x and y vorticities. Equation (4), together with the boundary conditions just discussed, define an eigenvalue problem for σ, with α and β as parameters. Equations (4a, b) define a linear operator on the space of vector fields (ω_x, ω_y) satisfying the vorticity boundary conditions; (4c–e) serve as subsidiary relations to enable the computation of z vorticity and velocity from the specified x and y vorticity. It is this operator which we will represent numerically in § 3.

Before continuing to the numerical solution, we will point out some important symmetry properties inherent in (4). First, we note that an eigenfunction belonging to σ for wavenumber β can be turned into an eigenfunction for $-\beta$ belonging to the same eigenvalue by simply reversing the sign of V_y and making the appropriate resulting changes in the x and z vorticity; hence, it is only necessary to consider positive values of β. Similarly, by reversing the sign of β and V_y and taking the complex conjugate of (4), we can construct an eigenfunction belonging to σ^* and $-\alpha$ from one belonging to σ and α, so that only positive α need be considered. These symmetries arise because there is no preferred y direction in the base state, and because the stability equations are derived from a system with only real coefficients. To progress further, we define the x and z parity inversion operators, whose action on the velocity field is given by

$$P_x: (V_x, V_y, V_z)[x, z) \to (-V_x, V_y, V_z)[\tfrac{1}{2}\pi - x, z]; \tag{6a}$$

$$P_z: (V_x, V_y, V_z)[x, z] \to (V_x, V_y, -V_z)[x, -z]. \tag{6b}$$

The associated transformations of vorticity should be clear. Now, it is easily but tediously verified that, from an eigenmode belonging to (σ, α, β), we can construct an eigenmode belonging to $(-\sigma^*, \alpha, \beta)$ by taking the complex conjugate, reversing the sign of V_y, and applying P_x. In the parallel flow case, this property reduces to the

familiar property that if complex phase velocity c is an eigenvalue of the Rayleigh problem, so is c^*, since $c = i\sigma/i\alpha$ in this limit. In deriving the general property, we have made use of the assumed x symmetry of Ω. The symmetry of Ω in z leads to an additional property, namely that we obtain an eigenmode belonging to $(-\sigma, \alpha, \beta)$ by applying P_z to an eigenmode belonging to (σ, α, β). These last two properties are essentially a consequence of the reversibility of the Euler equations, and would not obtain if viscous terms had not been discarded. The parity inversion properties imply that eigenvalues appear in groups $\pm\sigma$, $\pm\sigma^*$. This has the important consequence that for every exponentially damped mode there is a corresponding exponentially growing mode. Hence, the base state can be at best neutrally stable in a given parameter range. Further implications of the inversion properties for the manner in which instabilities set in or vanish will be discussed in § 6. There is a final symmetry which obtains when $\alpha = 0$. In this special case, $P_x P_z$ maps an eigenfunction for (σ, α, β) to another eigenfunction for (σ, α, β). This implies that modes for $\alpha = 0$ can be chosen to be simultaneous eigenmodes of $P_x P_z$, i.e. that they can be chosen to be symmetric or antisymmetric through the vortex centre (marked P in figure 1).

3. Numerical solution by spectral method

Our main task here is to approximate the linear operator implicitly defined in $(4a, b)$ by a finite-order matrix, whose eigenvalues can then be found using conventional methods. We will accomplish this by using a variant of the spectral-collocation technique. The use of this method for one-dimensional eigenvalue problems has been described by Boyd (1978), and its extension to the two-dimensional case is entirely straightforward. The use of collocation enables the discretization of the operator with a minimum of analytical effort, while retaining the high-order accuracy of a spectral method. In addition, the use of collocation to determine the matrix elements eliminates any reason for preferring orthogonal basis functions, leaving considerable freedom to choose functions automatically satisfying the boundary conditions.

Equations $(4a, b)$ can be represented in the schematic form

$$\mathscr{L}\begin{pmatrix}\omega_x\\ \omega_y\end{pmatrix} = \sigma\begin{pmatrix}\omega_x\\ \omega_y\end{pmatrix}, \tag{7}$$

where $\mathscr{L}$ is the 2×2 matrix of operators we wish to represent. We will denote 2-vector fields of the sort operated on by $\mathscr{L}$ with underlined symbols. With this notation, suppose that the vector fields $\underline{E}_n(x, z)$, $n = 0, \ldots, N$, form a complete set of basis functions for the space of x–y vorticity fields satisfying the vorticity boundary conditions, in the limit $N \to \infty$. Then, for large N, the horizontal vorticity field can be approximated uniquely by an expansion of the form

$$\underline{\omega} = \sum_{n=0}^{N} a_n \underline{E}_n(x, z). \tag{8}$$

To compute the matrix elements of $\mathscr{L}$, we need two general procedures. The first procedure ('back transformation') accepts as input the values on a finite grid (x_j, z_k) of a field f satisfying the vorticity boundary conditions, and produces as output the coefficients f_n in an expansion of the form in (8). The second procedure ('evolution') accepts as input the values of a field g on the grid, and produces as output the values

of $\mathscr{L}\underline{g}$ on the grid. With these two procedures, we can numerically compute the coefficients b_{mn} in the expansion

$$\mathscr{L}\underline{E}_m(x_j, z_k) = \sum_{n=0}^{N} b_{mn}\underline{E}_n(x_j, z_k) \quad \text{for} \quad m = 0, \ldots, N \tag{9}$$

by first using the evolution procedure to compute the left-hand side for each m, and then using the back transformation procedure to compute the coefficients on the right-hand side. Then, b_{mn} is the desired matrix approximation, since substitution of (8) into (7) and matching coefficients of $\underline{E}_n$ results in the finite-order matrix eigenvalue problem

$$\sum_{m=0}^{N} a_m b_{mn} = \sigma a_n \quad \text{for} \quad n = 0, \ldots, N. \tag{10}$$

In order to carry out this computation, we need to specify the expansion functions, derive the back transformation procedure, and derive the evolution procedure.

Considerable savings in time for the computation of b_{mn} result from defining the $\underline{E}_n$ in terms of separable functions of x and z. A truncated general expansion of $\underline{\omega}$ satisfying the conditions of vanishing vorticity at $z = \pm d$ and periodicity is given by

$$(\hat{\mathbf{x}}\omega_x + \hat{\mathbf{y}}\omega_y) = \sum_{m=0}^{N_x}\sum_{n=1}^{N_z} (\hat{\mathbf{x}}A_{mn} + \hat{\mathbf{y}}B_{mn})\, P_m(x)\, Q_n(z) + \sum_{m=0}^{N_x} A_{m0} Q_0(z)\, (i\beta\hat{\mathbf{x}} - \hat{\mathbf{y}}(i\alpha + \partial x))\, P_m(x), \tag{11}$$

where the $P_m(x)$ are periodic and complete in the space of periodic functions, the $Q_n(z)$ vanish at $z = \pm d$ and are complete in the space of functions that do so, and the Q_n satisfy the additional condition that

$$\int_{-d}^{d} dz\, Q_n(z) = \delta_{n0}. \tag{12}$$

This condition and the form of (11) are dictated by the constraint on vanishing z vorticity at the upper and lower boundaries in conjunction with (4c). This form of expansion implies vanishing mean component of perturbation y vorticity when $\alpha = 0$, and vanishing mean x component when $\beta = 0$, however; by integrating (4a, b) over one period in x and from $z = -d$ to $z = d$, it is found that the mean components vanish under the stated conditions unless $\sigma = 0$. Hence, as α or β is continuously varied, the expansion becomes possibly inadequate only at those points where $\sigma = 0$ exactly, and these isolated points can be located using interpolation. Further, the expansion places no constraints on the behaviour of the mean components in the limit $\alpha \to 0$ or $\beta \to 0$, since the coefficients A_{m0} are free to become arbitrarily large as zero is approached.

In order to carry out the back transformation, we define collocation points

$$x_1, \ldots, x_{N_x+1} \quad \text{and} \quad z_1, \ldots, z_{N_z+1};$$

if these points are suitably chosen, the square matrices $P_m(x_j)$ and $Q_n(z_k)$ will be invertible, with inverses defined so that

$$\sum_{j=1}^{N_x+1} P_m(x_j)\, P^{-1}_{jm_1} = \delta_{mm_1} \tag{13a}$$

and

$$\sum_{k=1}^{N_z+1} Q_n(z_k)\, Q^{-1}_{kn_1} = \delta_{nn_1}. \tag{13b}$$

Invertibility obviously requires $|x_{N_x+1}-x_1| < L$ and $-d < z_1 < z_{N_z+1} < d$, since otherwise two columns of the **P** and **Q** matrices vanish or are linearly dependent. With these definitions, the coefficients of the non-mean part are immediately found to be

$$A_{mn} = \sum_j \left(\sum_k \omega_x(x_j, z_k)\, Q^{-1}_{kn}\right) P^{-1}_{jm}, \tag{14a}$$

$$B_{mn} = \sum_j \left(\sum_k \omega_y(x_j, z_k)\, Q^{-1}_{kn}\right) P^{-1}_{jm}, \tag{14b}$$

where $n \neq 0$. Note that, because of the separable expansion, the back transformation requires only $O((N_x+1)^3+(N_z+1)^3)$ operations rather than $O((N_x+1)^3(N_z+1)^3)$, which represents a substantial saving in operation count. The determination of the A_{m0} components is almost equally straightforward. By integrating (11) from $z=-d$ to $z=d$, using (12), and taking the z-component of the curl of the resulting equation, we obtain

$$(i\alpha+\partial_x)\,\bar{\omega}_y - i\beta\bar{\omega}_x = \sum_{m=0}^{N_x} (\beta^2-(i\alpha+\partial_x)^2)\, P_m(x)\, A_{m0}, \tag{15}$$

where overbars indicate quantities integrated in z. The A_{m0} components are then found from (15) by inverting the matrix

$$M_{mj} = (\beta^2-(i\alpha+\partial_x)^2)\, P_m(x_j). \tag{16}$$

In the special case, $\alpha=\beta=0$, the row M_{0j} vanishes (assuming we have chosen $P_0 = \text{const.}$), leaving A_{00} indeterminate. As we have already discussed, when $\alpha=\beta=0$, the mean component in the expansion is nugatory; hence, the row of **M** corresponding to $m=0$ can be neglected, and the remainder of the matrix inverted on the space of functions with vanishing x means in this special case. In general, this restricted inverse could be computed by neglecting the column of **M** corresponding to one given collocation point (say, $x_{\frac{1}{2}N_x}$), but, for the simple Fourier basis functions we will choose for **P**, it is possible to effect the inversion analytically. The evaluation of the x derivative appearing on the left-hand side of (15) will be discussed shortly.

Since the P_m need only be complete and periodic, a logical choice is

$$P_m(x) = \begin{cases} \cos(2mx), & m \text{ even}, \\ \sin(2((m+1)/2)\,x), & m \text{ odd}, \end{cases} \tag{17}$$

with associated collocation points given by

$$x_j = j\frac{\pi}{N_x+2}, \quad j = 1, 2, \ldots, N_x+1. \tag{18}$$

We have chosen sines and cosines rather than complex exponentials so as to make the basis functions parity eigenfunctions. The choice of the Q_n is only slightly more complicated. It is convenient to carry out the z expansion in terms of Tschebychev polynomials. For generality, we introduce a stretched variable $r \in [-1, 1]$ defined by

$$z = d\frac{\tanh^{-1}(\lambda r)}{\tanh^{-1}(\lambda)}, \tag{19}$$

where $\lambda \in [0, 1]$. For λ near zero, the mapping is approximately linear, whereas, for λ near unity, an evenly spaced set of points z_j is mapped to a set of points r_j clustered near ± 1. This variable stretching is necessary because Tschebychev polynomials vary

most rapidly for argument r near ± 1, whereas the steady shear layer varies most rapidly near $z = 0$. Now, let $T_n = T_n(r)$ be the nth Tschebychev polynomial of argument r, and let $r' = dr/dz$, so $dz = dr/r'$. Then, we can satisfy the requirements set for Q_n by taking

$$Q_0(z(r)) = \frac{T_0 - T_2}{\int_{-1}^{1} dr\,[(T_0 - T_2)/r']} \tag{20a}$$

and, for $n > 0$,

$$Q_n(z(r)) = \begin{cases} T_0 - T_{n+4} - c_n Q_0, & n \text{ even}, \\ T_1 - T_{n+2}, & n \text{ odd}, \end{cases} \tag{20b}$$

where

$$c_n = \int_{-1}^{1} dr\,[(T_0 - T_{n+4})/r']. \tag{20c}$$

Note that Q_n is symmetric in z for n even and antisymmetric for n odd. A suitable set of collocation points, in light of the definition of the Tschebychev polynomials, is given by

$$r_k = -\cos\left(k\frac{\pi}{N_z + 2}\right), \quad k = 1, \ldots, N_z + 1. \tag{21}$$

The above discussion has implicitly defined the basis functions E_n and the back transformation procedure. It remains to specify the evolution procedure. This involves: numerical x differentiation to compute the right-hand side of (4c), numerical z integration to solve (4c) for ω_z, solution of the three independent elliptic equations for Ψ stated in (4d) and (5), differentiation to find the velocity field via (4e), and finally differentiation to compute the vorticity gradients appearing in the left-hand sides of (4a, b). The technique of pseudo-spectral differentiation and integration is by now well known (see Gottlieb & Orszag 1977). In the collocation variant, one finds the x derivative of a function $f(x)$ tabulated on points x_j by expanding f in functions $P_m(x)$ using (13a), taking the x-derivative of each P_m analytically, and transforming back to x-space, so that the derivative is given by

$$\left.\frac{df}{dx}\right|_{x_j} = \sum_m f_m P'_m(x_j). \tag{22}$$

Similarly, a function $g(r)$ can be differentiated with respect to r by expanding in Tschebychev polynomials $T_n(r)$ and substituting their derivatives before transforming back to r-space. To integrate with respect to r, the integrals of $T_n(r)$ are substituted instead. The z derivatives and integrals can then be computed using the relations $dg/dz = r'\,dg/dr$ and $\int g\,dz = \int (g/r')\,dr$. To solve the elliptic equation

$$(\partial_{zz} - \beta^2 + (i\alpha + \partial_x)^2)\,\Psi = F(x, z) \tag{23}$$

we first expand the right-hand side in a series

$$F = \sum_{m=-\frac{1}{2}N_x}^{\frac{1}{2}N_x} F_m(z)\, e^{2imx} \tag{24}$$

using collocation, and assume an expansion of the form

$$\Psi = \sum_{m=-\frac{1}{2}N_x}^{\frac{1}{2}N_x} \sum_{n=0}^{N_z} \Psi_{mn}\, e^{2imx} S_{mn}(z). \tag{25}$$

The S_{mn} are chosen to be complete in the space of functions satisfying the boundary condition given in (5), so that we need

$$\partial_z S_{mn}|_{z=\pm d} = \mp \gamma_m S_{mn}(\pm d). \tag{26}$$

Letting $r'_d = r'|_{z=d}$, we can satisfy this requirement with

$$S_{mn}(z) = \begin{cases} d^{(1)}_{mn} T_n(r) + d^{(2)}_{mn} T_{N_z+2}(r), & n \text{ even}, \\ d^{(1)}_{mn} T_{n+2}(r) + d^{(2)}_{mn} T_1(r), & n \text{ odd}, \end{cases} \tag{27}$$

where

$$d^{(1)}_{mn} = -(r'_d T'_{N_z+2}(1) + \gamma_m T_{N_z+2}(1)), \quad d^{(2)}_{mn} = r'_d T'_n(1) + \gamma_m T_n(1) \tag{28}$$

for n even, and

$$d^{(1)}_{mn} = -(r'_d + \gamma_m), \quad d^{(2)}_{mn} = r'_d T'_{n+2}(1) + \gamma_m, \tag{29}$$

for n odd. In these relations, we have assumed N_z even. Ψ is known from (25) if Ψ'_{mn} is known; to compute the latter, we substitute (25) and (24) into (23), and write the resulting equation at the collocation points $z_1, \ldots, z_{N_z+1}$ defined as before. This results in the equation

$$\sum_{n=0}^{N_z} \Psi'_{mn} \left(\frac{d^2 S_{mn}}{dz^2} - \gamma_m^2 S_{mn} \right)\Big|_{z=z_k} = F_m(z_k). \tag{30}$$

Hence, the Ψ'_{mn} may be found by inverting the $N_x + 1$ matrices

$$C^{(m)}_{nk} = \left(\frac{d^2 S_{mn}}{dz^2} - \gamma_m^2 S_{mn} \right)\Big|_{z=z_k}. \tag{31}$$

These matrix elements are most conveniently computed numerically using spectral z-differentiation. The matrices need be computed and inverted only once for each choice of α and β, a process that requires only $O((N_x)(N_z)^3)$ operations. Once the inverses have been computed, each solution of (23) requires a further $O((N_x)(N_z)^2)$ operations. When $\alpha = \beta = 0$, the row $C^{(0)}_{0k}$ vanishes, since $\gamma_0 = 0$ and $S_{00} = \text{const.}$ in this case. This is just a reflection of the fact that Ψ is physically indeterminate to the extent of addition of a constant when $\alpha = \beta = 0$; the inversion can be made unique by dropping the S_{00} term from (25) and eliminating one collocation point from (31). Solvability of (23) when $\alpha = \beta = 0$ is guaranteed because the mean components of perturbation vorticity vanish in this limit.

The procedure to compute one row of the discretized matrix may be summarized as follows:

(1) Pick a basis function appearing in the expansion given in (11). This determines $\omega_x(x_j, z_k)$ and $\omega_y(x_j, z_k)$.

(2) Compute the right-hand side of (4c) and find ω_z by spectral integration.

(3) From $\omega_x, \omega_y, \omega_z$ compute Ψ_x, Ψ_y, Ψ_z, by solving (4d).

(4) Compute the velocity field V_x, V_y, V_z, from (4e), using spectral differentiation.

(5) Substitute $V_x, V_y, V_z, \omega_x, \omega_y, \omega_z$, into (4$a$, b), and determine the values of the left-hand side on the collocation grid.

(6) Using the back-transformation procedure, numerically express the 2-vector field resulting from the previous step in an expansion of the form of (11). These coefficients constitute the desired row.

This procedure is repeated until all the basis functions appearing in (11) are exhausted. The procedure is equivalent to computing the time rate of change of a

complete set of initial conditions for ω_x and ω_y. When $\alpha = 0$, the eigenfunctions can be chosen to have definite parity, so that the matrix splits into two independent submatrices: one corresponding to ω_y even and ω_x odd, and the other corresponding to ω_y odd and ω_x even. When $\beta = 0$, the eigenfunctions also split into two classes: the first with $\omega_y = 0$ and the second with $\omega_x = 0$. The latter class of modes is physically two-dimensional, as the modes lack a y-velocity component.

The procedure outlined above results in an $N \times N$ complex general matrix, whose eigenvalues are to be found numerically; $N \simeq N_x N_z$ for $\alpha = 0$, and $N \simeq 2N_x N_z$ otherwise. Computation of the matrix elements requires $O(N_x^2 N_z^3)$, while computation of the eigenvalues by reduction of the matrix to Hessenberg form and subsequent application of the LR algorithm requires $O(N^3) = O(N_x^3 N_z^3)$ operations. This estimate indicates that the computation of the eigenvalues of the discretized matrix consumes the lion's share of the computational effort, and hence is the prime target for optimization. We ran our code on the 4-pipe Texas Instruments ASC at the NOAA Geophysical Fluid Dynamics Laboratory in Princeton, N.J. The ASC is capable of performing 48×10^6 single precision floating point operations per second, but attains this speed only when operating in vector mode, i.e. performing operations that can essentially be carried out in parallel. To take advantage of this feature, we rewrote the EISPACK (Smith *et al.* 1974) eigenvalue routines COMHES and COMLR so as to vectorize as completely as feasible. With these modifications, all the eigenvalues of a 120×120 double precision complex matrix could be found in 55 c.p.u. seconds. (A double-precision complex word on the ASC occupies 64 bits of storage.) The time required for computation of the matrix elements, by comparison, is under 10 % of this for $N_x = 6$ and $N_z = 8$. The cubic dependence of c.p.u. time on N underscores the necessity of using a spectral representation of the problem. Boyd (1978) estimates that typically four times as many grid points in each direction are needed for a finite-difference method to equal a spectral method in accuracy. This translates into a factor of 4096 difference in running time between a two-dimensional spectral and finite-difference algorithm of comparable accuracy.

The numerical method requires the specification of four approximation parameters: the height d of the computational domain, the variable stretching parameter λ, and the truncation numbers N_x and N_z. A value $d = 1{\cdot}5$ was found to be adequate; at this height, the steady-state vorticity falls to 1 % of its maximum value even in the worst case $\rho = 0$. In addition, it was experimentally determined that increasing d beyond this value produced only negligible changes in the eigenvalues computed. A value $\lambda = 0{\cdot}95$ was arrived at by solving numerically for the velocity field associated with vorticity $\partial_x \Omega$ for various ρ, and varying λ to obtain the best overall accuracy. N_x and N_z were determined on a case-by-case basis by studying the behaviour of the eigenvalues of interest as the truncation numbers were increased, and picking values of truncation numbers corresponding to convergence to graphical (usually two significant figure) accuracy. The convergence tests were generally continued to N_x and N_z both 1·5 times the 'converged' values. In many cases, the truncation numbers used for particular calculations to be reported were excessive, because it was convenient to use the same N_x and N_z for entire series of calculations.

4. Subharmonic instabilities: pairing and helical pairing

We turn first to the class of modes with $\alpha = 1$. Since $L = \pi$ these represent subharmonic modes, which repeat with a period $2L$ comprising two vortices. The physical modes (with the $e^{i\alpha x}$ phase factor multiplied back in) have the property that

$$f(x+L) = -f(x),$$

where f is any perturbation quantity. Thus, generally speaking, the subharmonic modes are modes in which adjacent vortices are displaced in opposite directions.

In figure 3, we show the growth rate of the most unstable mode with $\beta = 0$ as a function of the vortex core size parameter ρ. These modes represent two-dimensional disturbances to the two-dimensional base state. These calculations, as with all others to be discussed in this section, were carried out with $N_x = 4$ (5 modes in x direction) and $N_z = 6$ (7 modes in the z direction). In all cases considered, the most unstable mode was purely exponentially growing, i.e. $\sigma_i = 0$. For $\rho = 0$, the base state reduces to a parallel hyperbolic tangent shear flow, the stability properties of which have been summarized by Kelly (1967). We find a growth rate of 0·367 for the parallel case, which compares well with the growth rate of 0·369 reported by Kelly. It is noteworthy that the maximum growth rate in the parallel-flow case occurs at $\alpha = 0{\cdot}886$, so that the 'subharmonic' mode is nearly the most unstable even in the parallel case. As ρ is increased, the growth rate increases monotonically, and becomes asymptotic to a value $\sigma_r = 0{\cdot}5$. This asymptote has been essentially attained by $\rho = 0{\cdot}3$. Lamb's instability of a row of point vortices (Lamb 1932) has a growth rate of 0·5 when reduced to our units. Thus, the behaviour shown in figure 3 represents a smooth transition from parallel-flow-like instability to point-vortex-like instability. An important observation is that the asymptote is reached at moderate ρ, when the vortices are still relatively large. The mode shape provides further grounds for identifying the family of instabilities in figure 3 with an interaction of the pairing type. In figure 4, we show contour plots of perturbation y-vorticity (including the phase factor) over the stretch $x = 0$ to $x = L$, encompassing one unperturbed vortex. The eigenmode multiplied by the $e^{i\alpha x}$ phase factor can be chosen so as to be purely real. Therefore, the phase relationship between the subharmonic and the fundamental is not altered by multiplication by a complex constant, except possibly to the extent of an overall reversal of sign of the perturbation. The cross marks the centre of the unperturbed vortex, and regions of negative vorticity are indicated by shading. The most striking feature of this figure is the slanted nodal line passing through the unperturbed vortex centre. This structure indicates that the instability shifts the vortex up and to the right. The comparable plot between $x = L$ and $x = 2L$ is merely reversed in sign, and represents a shift of the vortex down and to the left. The net motion, then, resembles the beginning of a clockwise rotation of the vortex and its neighbour about each other.

The pairing interaction has been particularly well studied, beginning with its observation by Wille (1963). Browand & Weidman (1976) have measured vorticity contours of vortices in the process of pairing and arrived at a picture very like the mutual rotation described above, once it is observed that the higher-speed stream is represented as being at the bottom half of their figure 6(*b*), leading to counter-clockwise rotation. In addition, time scales for the completion of pairing can be estimated by relating the kinetics of pairing to the rate of shear-layer spread. Brown &

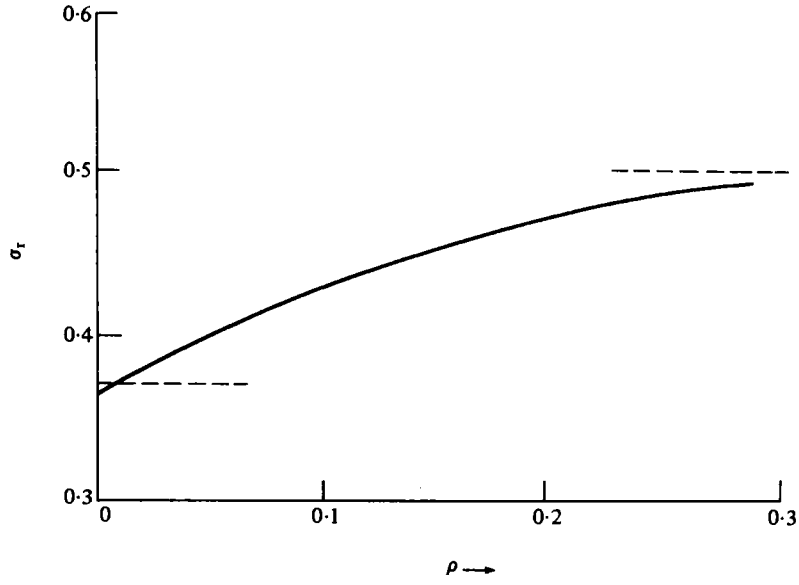

FIGURE 3. Dependence of growth rate of the two-dimensional pairing mode on the vortex core size parameter. $\rho = 0$ corresponds to a parallel hyperbolic tangent shear profile. The lower dashed line is the independently calculated growth rate for the instability of a hyperbolic tangent shear flow, while the upper represents the growth rate for the subharmonic instability of a row of point vortices, as given by Lamb.

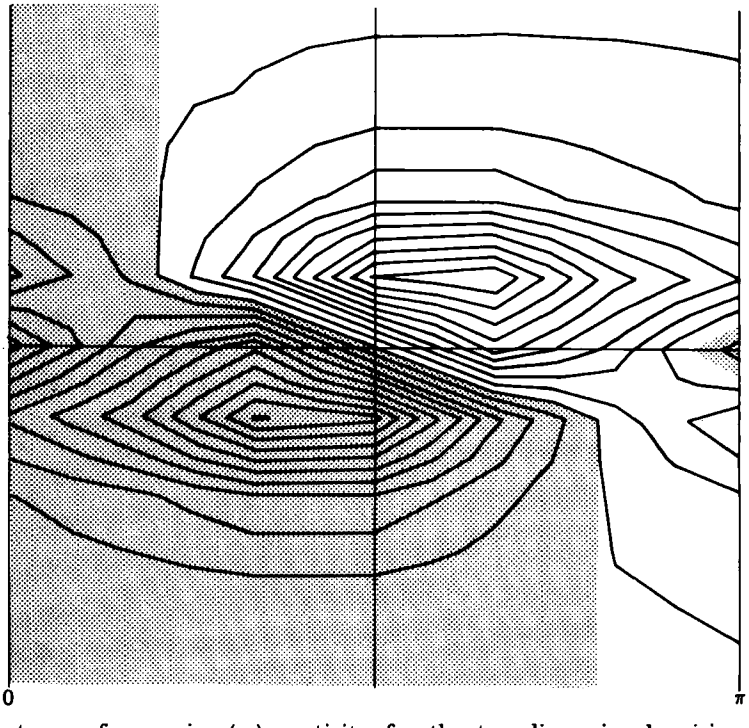

FIGURE 4. Contours of spanwise (y-) vorticity for the two-dimensional pairing mode with $\rho = 0{\cdot}2$. Shaded areas are regions of negative vorticity. The cross denotes the location of the centre of the unperturbed vortex. Only a half-period of the mode is shown.

Roshko (1974) used the Taylor hypothesis to derive such a relation; their (4.1) can be cast in the form

$$\frac{d\delta_\omega}{dx} = \frac{2}{\tau^*}\frac{U_1 - U_2}{U_1 + U_2}, \tag{32}$$

where τ^* is the characteristic time for vortex amalgamation by pairing, measured in units of local time scale $\delta_\omega/(U_1 - U_2)$ and δ_ω is the vorticity thickness. Brown & Roshko examined the rates of spread measured by numerous experimenters under varying conditions, and found that (32) fit the collected observations remarkably well. A value $\tau^* = 11{\cdot}11$ can be measured from their figure 10. At $\rho = 0{\cdot}25$, the e-folding time for the calculated pairing instability in the same local units is $\tau_e^* = 4{\cdot}08$; hence, the characteristic amalgamation time is 2·72 e-folding times, corresponding to an amplification factor of 15. Thus, the pairing instability has a time scale which could account for the observed rate of spread. Even more direct confirmation may be found in the work of Miksad (1972) who directly measured the growth rate of energy in the subharmonic component. From his figure 11, the subharmonic growth rate of r.m.s. velocity in the post-equilibrated phase can be calculated, and reduces to $\sigma_r = 0{\cdot}46$ in our units. This agrees very well with our growth rate $\sigma_r = 0{\cdot}49$ at $\rho = 0{\cdot}25$. In light of these comparisons, there is little reason to doubt that the pairing instability is the mechanism of subharmonic generation and shear-layer growth.

An alternative mechanism for shear-layer growth has been proposed by Moore & Saffman (1975*a*). This process, known as the tearing mechanism, relies on certain mathematical properties of the nonlinear steady states of the shear layer which we have confirmed elsewhere (Pierrehumbert & Widnall 1981). The tearing mechanism is a nonlinear process which is unrelated to the linear stability properties of the vortex row, and whose time scale depends on the rate of entrainment of irrotational fluid into the vortex cores by turbulent processes. It has not proved possible to make quantitative predictions of the time scale of this amalgamation process, but it is certain that the characteristic amalgamation time is sensitive to the degree of small-scale turbulence. Experimental evidence does not support such a dependence. In fitting (32), Brown & Roshko found similar values of amalgamation time over widely varying experimental conditions. Moreover, experiments varying unit Reynolds number (figure 20 in Brown & Roshko; figure 1 in Bernal *et al.*) demonstrate quite clearly that shear-layer growth is little affected by the level of small-scale turbulence. It thus seems that tearing does not play a central role in determining the dynamics of shear-layer growth, although it may still play some part in determining the size of the vortices.

We turn now to the behaviour of the modes shown in figure 3 when $\beta > 0$, so that the modes have spanwise variations. In figure 5, we show the growth rates as a function of β for various values of ρ. Significantly, the pairing instability is always most unstable in the two-dimensional case $\beta = 0$, and has a short-wave cutoff in β. Convergence of the expansion near the stability boundaries was very slow, so the numerical accuracy of the critical wavenumbers for stability is somewhat in doubt. As ρ is increased, the short-wave cutoff first increases to $\beta = 3$ at $\rho = 0{\cdot}1$, and thereafter decreases again as ρ is further increased, reaching a value $\beta = 2{\cdot}2$ at $\rho = 0{\cdot}25$. This behaviour is the result of two competing effects: Initially, increasing ρ produces a thin, flat vortex structure which acts somewhat like a thinner shear layer than the original one, and

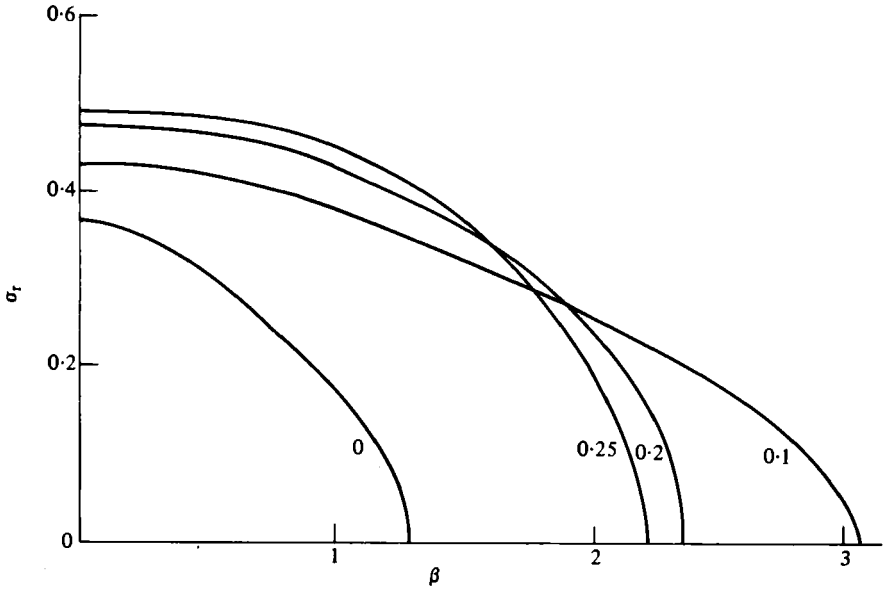

FIGURE 5. Growth rates for helical pairing as a function of spanwise wavenumber. Numbers on curves give values of ρ.

can therefore support smaller-scale instabilities. As ρ is increased further, however, the vorticity is gathered up into a compact core, and the stabilizing effects of self-induced vortex tube rotation begin to become important. The y-vorticity cross-section of the mode is similar to figure 4, except that the nodal plane becomes more horizontal as the cutoff is approached. Since the modes for (σ, β) and $(\sigma, -\beta)$ differ only in the sign of $\tilde{V}_y$, we can superpose solutions for $\pm\beta$ to obtain planar modes of the form

$$\left.\begin{aligned}\omega_y(x,y,z,t) &= e^{\sigma t}\,\mathscr{R}(\tilde{\omega}_y\, e^{i\alpha x})\cos(\beta y),\\ \omega_x(x,y,z,t) &= e^{\sigma t}\,\mathscr{R}(i\tilde{\omega}_x\, e^{i\alpha x})\sin(\beta y).\end{aligned}\right\} \tag{33}$$

For these modes, the perturbed vortex cores lie in parallel planes intersecting the plane $z = 0$ along the lines $x = \frac{1}{2}L, 3L, 5L, \ldots$. Because of the subharmonic dependence on x, neighbouring vortex cores are shifted alternately above and below the plane $z = 0$. We have depicted this situation in figure 6, annotating points above the plane with a $+$ and below the plane with a $-$. The displacements of the vortex tubes have been exaggerated for purposes of clarity. For linear theory to be valid, the displacements of the vortex cores would have to remain small compared to the core size. From this figure, it is clear that if nonlinear effects do not drastically alter the character of the instability as it grows the instability would result in pairing of the middle vortex tube with its upstream neighbour at spanwise stations $\beta y = -\pi, \pi, 3\pi, \ldots$, and with its downstream neighbour at $\beta y = 0, 2\pi, \ldots$. This process would result in phase dislocations in the spanwise direction, and the generation of coherent three-dimensional structures with a typical scale $\beta(\Delta y) = \pi$. The existence of a sharp short-wave cutoff for this type of instability has an interesting implication for its behaviour in the context of spatial development of a shear layer. In dimensional form, the short-wave cutoff implies that spanwise scales with $\beta\delta_\omega >$ const. do not amplify as they advect downstream. Thus, as debris of a given scale produced by an instability at x_0 moves to

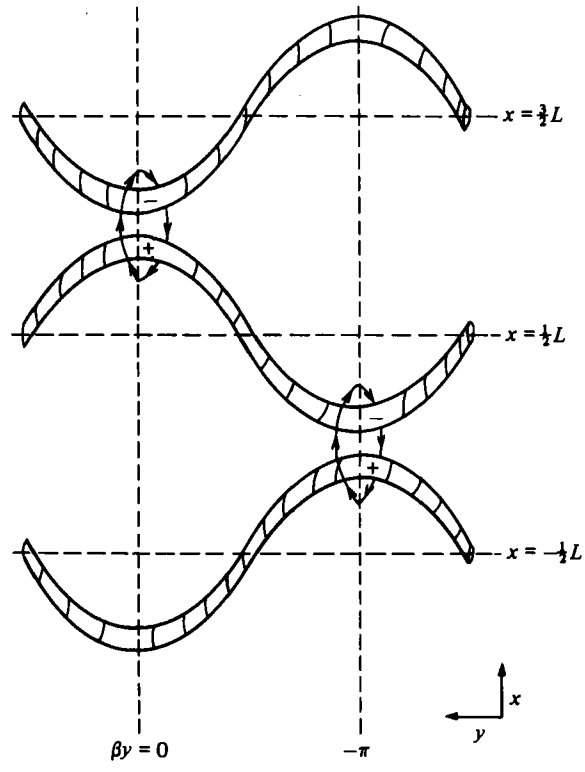

FIGURE 6. Three-dimensional structure of helical pairing. Points annotated with a + are displaced upward, while those with a − are displaced downward. Circled regions are regions of localized pairing. The state shown is an extrapolation of the effects of the instability beyond the range in which linear theory is valid.

larger x, it will eventually pass the short-wave cutoff and cease to grow, since δ_ω is continually increasing downstream. This effect limits the extent to which localized pairing can disrupt the large-scale two-dimensional structure, particularly since the two-dimensional pairing instability is more vigorous than its three-dimensional relatives, and can therefore increase the shear-layer thickness by pairing before the three-dimensional instability can get very far.

Chandrsuda *et al.* (1978) have directly observed generation of spanwise phase dislocations via localized pairing, and given the process the name 'helical pairing'. We will continue this terminology, although the localized pairing instability we have discussed is made up of planar vortex waves rather than helical ones. (The instability is helical in the sense that it causes neighbouring vortex tubes to twist around one another.) The long-wave nature of helical pairing has been experimentally confirmed by Chandrsuda *et al.*; moreover, the flow pattern shown in their figure 3 bears a resemblance to the mode shape we have depicted in figure 6. Generation of branching vortices has been observed in experiments by Browand & Troutt (1980) and in numerical simulations by Mansour, Ferziger & Reynolds (1978). Browand & Troutt (1980) have measured velocity correlation as a function of spanwise separation of the velocity probes, and concluded that the shear layer reaches an asymptotic state composed of large-scale structures with a typical spanwise scale of 2·3 times the local vorticity

thickness. Wygnanski *et al.* (1979) observed similar values of the spanwise correlation scale, although they did not verify that an asymptotic state had been reached. In our units, this scale corresponds to a wavenumber $\beta = 1{\cdot}4$, which according to figure 5 is capable of moderately rapid growth when $\rho = 0{\cdot}25$. Browand & Troutt find that the beginning of the asymptotic self-similar regime corresponds to the completion of the second vortex pairing, which is consistent with the time scales involved in helical pairing. Thus, it is plausible that the three-dimensional structures observed in the shear layer are at least partly due to the helical pairing instability. However, as we will discuss in the next section, there is another instability which can generate three-dimensional structures, and which may also contribute to the observed correlation patterns.

5. Fundamental mode instabilities: the onset of streamwise streaks

In addition to the subharmonic family of instabilities, there is a family of fundamental mode instabilities with $\alpha = 0$, which repeat in x with the same periodicity as the undisturbed vortex row, so that adjacent cores move in the same direction. Modes with $\alpha = 0$ split into two subclasses: those with ω_y antisymmetric through the vortex centre and those with ω_y symmetric through the vortex centre. We have found appreciable instability only for modes of the former class, which correspond to net translation of the vortex cores rather than bulging.† In figure 7, we show the growth rates for the fundamental mode instability as a function of β for $\rho = 0{\cdot}1$ and $\rho = 0{\cdot}25$. The calculations were carried out with $N_x = 8, N_z = 8$. The modes have purely exponential growth, and the growth rate falls to zero linearly as $\beta \to 0$. We have found that the steady perturbation which the mode reduces to in the two-dimensional limit represents an infinitesimal translation of the vortex row, which of course yields another steady solution; for this reason, we will refer to the instability as the 'translative instability'.

The translative instability, unlike the pairing instability, is not an extension of any instability occurring on a parallel shear layer. In the parallel case ($\rho = 0$), the curves shown in figure 7 fall identically to zero, and the mode represents a parallel flow perturbation to the initial parallel shear layer, which has the effect of moving the shear layer up or down at different spanwise stations while leaving it parallel. As ρ is increased, the maximum growth rate increases and the most unstable wavenumber moves out from zero. At $\rho = 0{\cdot}25$, the maximum growth rate is 0·46, somewhat less than that of the two-dimensional pairing instability, and occurs near $\beta = 3$, representing a spanwise wavelength $\frac{2}{3}$ of the spacing to the undisturbed vortices. An important feature of the instability is that the growth rate decreases only slowly from its maximum value as the wavenumber is increased. This means that the instability suffers little 'detuning' as the thickness of the shear layer grows. From figure 7, it can be seen that the translative instability for $\rho = 0{\cdot}25$ can survive and grow through at least three doublings of shear-layer thickness (pairings) before its growth rate is appreciably reduced.

In figure 8, we show contours of perturbation y-vorticity for $\beta = 2, \rho = 0{\cdot}25$. As with the pairing instability, the translative mode shifts the vortex up and to the right, into

† *Note added in proof:* Two-dimensional fundamental modes ($\alpha = 0$, $\beta = 0$) were never found to be unstable.

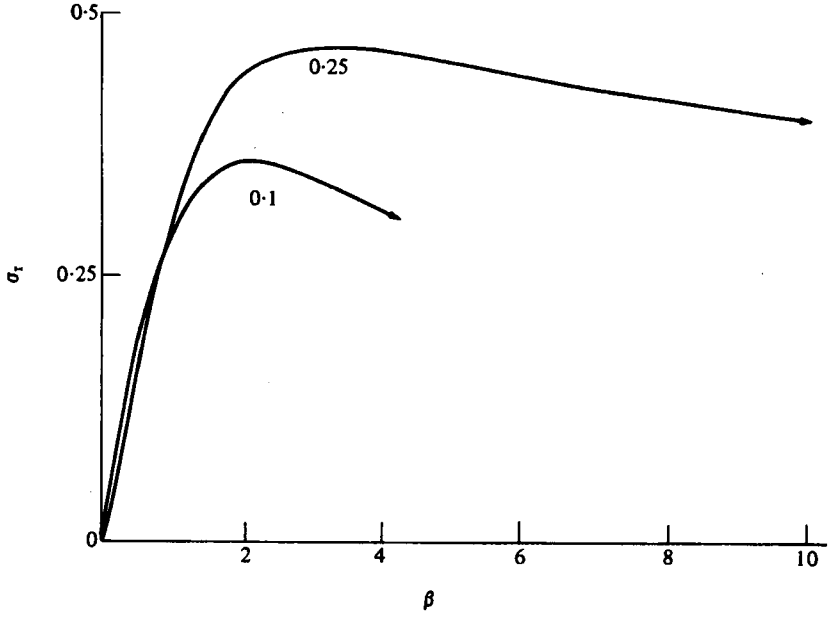

FIGURE 7. Growth rates of the translative instability of a periodic shear layer, as a function of axial wavenumber. Numbers on curves give values of core size parameter.

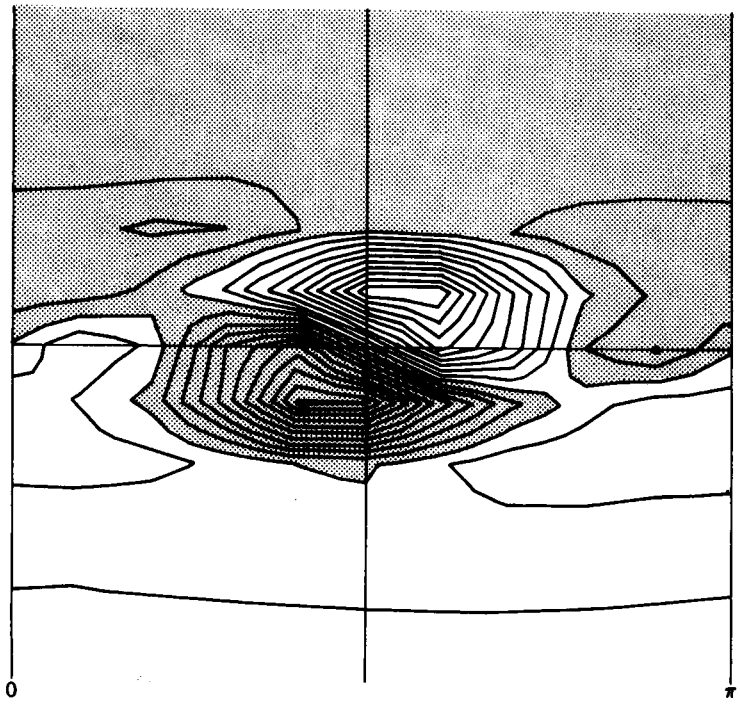

FIGURE 8. Same as figure 4, but for the translative instability. A full period is shown in this case.

the free stream, although the translative instability is rather more localized in the vortex core than was pairing. Neighbouring vortices in the translative instability are of course shifted in the same direction. This description represents the behaviour at only one spanwise station. The three-dimensional structure is given by (33) with $\alpha = 0$; ω_y, and hence the vortex shift, has nodes at $y = \frac{1}{2}\pi, \frac{3}{2}\pi, \ldots$, whereas the streamwise vorticity ω_x has maxima at these values. The vortex tube is shifted up into the fast stream at $\beta y = 0, 2\pi, \ldots$, and down into the slow stream at $\beta y = -\pi, \pi, \ldots$. This situation is depicted in figure 9. As in figure 6 the vortex tube displacements have been extrapolated beyond the range in which linear theory is valid. Under the assumption that nonlinearity does not alter the fundamental character of the instability, we can offer some speculations as to the evolution of the flow after the translative instability sets in. As the instability progresses, a loop of vortex tube at $y = 0$ is lifted up into the free stream and stretched out. Through tilting of the vortex tube, a sizable streamwise vorticity component is generated at the points marked P in the figure. The streamwise vorticity takes the form of a pair of counter-rotating streamwise vortices with a region of upwelling in between. The upwelling regions occur at spanwise intervals of $2\pi/\beta$.

For $\rho = 0{\cdot}25$, the spanwise wavelength associated with the translative instability is about half that characteristic of helical pairing. This scale is smaller than the scale implied by the spanwise correlation experiments reviewed in the previous section. Moreover, the broad wavenumber range in which the translative instability occurs does not reflect the definite scaling of observed correlation length with local vorticity thickness as well as does the helical pairing mode. There is a degree of arbitrariness in the comparison of instability scales with correlation lengths, and it is therefore difficult to say with certainty the degree to which the translative instability is connected with the observed large-scale three-dimensional structures as reflected in the correlation measurements. However, there is a phenomenon occurring in the shear layer which seems to correspond to the translative instability. This phenomenon is the streaky structure observed by Breidenthal (1978) and by Bernal *et al.* (1979). The streaks set in with a spanwise spacing somewhat less than the wavelength of the initial Kelvin–Helmholtz instability; this is consistent with the properties of the translative instability, as the translative instability has a growth rate comparable to that of the pairing instability, so that it should set in simultaneously with the first pairing. This picture is also supported by the earlier work of Miksad (1972), who reported that the region of subharmonic growth following equilibration of the initial Kelvin–Helmholtz instability is coincident with the region of initial generation of three-dimensionality. Like the translative instability, the streak pattern survives and grows through several pairings with little change in scale. The following description, from Bernal *et al.* (1979), underscores the resemblance to the translative instability: 'The streaks sometimes originate from a sinusoidal pattern that develops in the spanwise vortices which emerge from the Kelvin–Helmholz instability. Amplification of the pattern's amplitude, possibly due to straining, as it convects downstream with the vortices tends to stretch out the streamwise oriented segments of the pattern; the streaks apparently result from this stretching.' In figure 11 of Breidenthal (1978) a possible instance of this development is shown. The wavy pattern is visible on three adjacent vortex tubes, and the basic characteristics of the translative instability are evident: (1) The pattern is coherent in phase over the three vortices, so that the

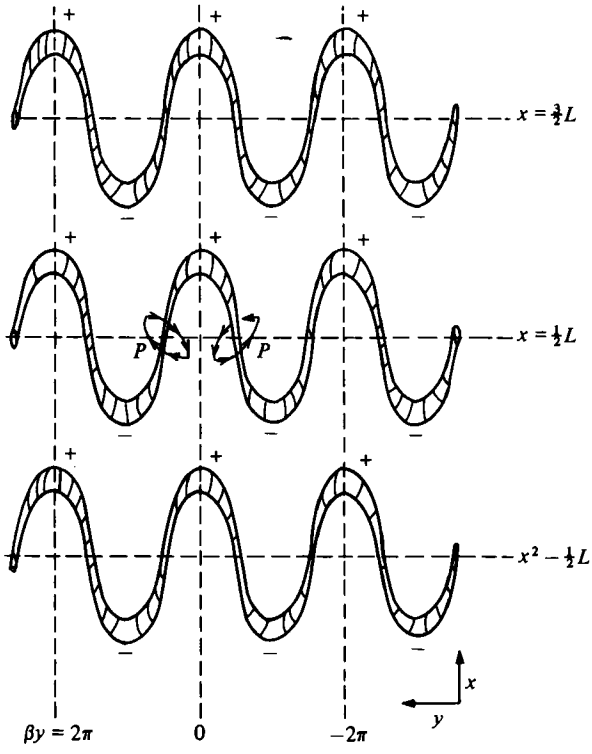

FIGURE 9. Three-dimensional structure of the translative instability of a periodic shear layer. As with figure 6, the state shown represents an extrapolation to a highly nonlinear regime.

crests line up, (2) the wavelength is shorter than the vortex spacing and doesn't change downstream, and (3) the instability is most visible in the central regions of the vortices, and an outer envelope of relatively undisturbed fluid is faintly visible.† In addition, the characteristic streamwise counter-rotating vortices and regions of upwelling have been directly observed by Bernal *et al.* (1979) in independent experiments. We note in passing that the instability does not mark the end of the organized structure of the shear layer; the experiments indicate that the instability leads to the generation of small-scale turbulence and increased mixedness, but leaves the large-scale structure relatively intact.

6. Higher-order modes

Besides the instabilities discussed above, there are also a number of three-dimensional instabilities of a periodic shear layer which have a more complicated modal structure. These modes all have weaker growth rates than the pairing and translative modes, and are generally oscillatory ($\sigma_i \neq 0$). We show the family of eigenvalues for one such mode in figure 10. The family consists of a pair of neutrally stable oscillations at $\beta = 0$, whose frequencies become degenerate at some finite value of β. Past this point, the frequencies coalesce and the growth rate increases from zero. The

† Dimotakis (1980, personal communication), however, has pointed out certain possible ambiguities in the connection between the dark dye regions in Breidenthal's photograph and displaced vortex cores. Additional experimental work is required to resolve this ambiguity.

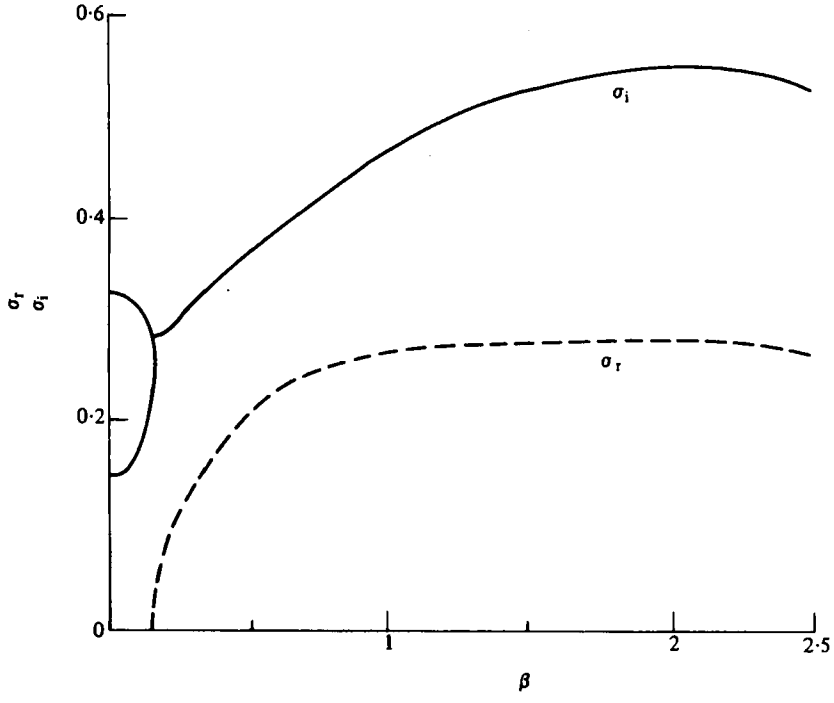

FIGURE 10. Onset of instability for a typical higher-order mode, with $\alpha = 1$, $\rho = 0{\cdot}2$. The solid lines in this case give the imaginary parts of the eigenvalues, while the dashed line gives the growth rate.

number of eigenvalues remains constant in this process, as we begin with two eigenvalues $\sigma = i\sigma_i^{(1)}$, $i\sigma_i^{(2)}$ and end with two eigenvalues $\sigma = \pm\sigma_r + i\sigma_i$. This process of transition through degeneracy is reminiscent of the onset of short-wave instabilities on a weakly strained vortex tube, as discussed by Tsai & Widnall (1976). In fact, this sort of transition from neutral stability to instability is to be expected in any inviscid system, since unstable eigenvalues for such systems are always born in pairs with real parts $\pm\sigma_r$. This means that, insofar as the system can be represented as a finite-order matrix with non-degenerate eigenvalues, two neutrally stable eigenvalues must coalesce at the transition point in order to prevent the number of eigenvalues after the transition point from exceeding the order of the matrix.

Because the higher-order modes involve rather small scales, they are more sensitive to numerical inaccuracy and inaccuracy of the physical model taken for the shear layer; hence, we are reluctant to draw comparisons with the observations, even though some of the calculated growth rates would be large enough to produce measurable effects. Nevertheless, the existence of higher-order instabilities in the mathematical model indicates that something similar may occur in the physical situation.

7. Conclusions

We have found that an instability calculation based on a reaslitic model of the observed vortical structure of the free shear layer can reproduce certain features of a number of stages in the development of the shear layer. There are two main classes of instability: subharmonic and translative. The subharmonic instability has its

greatest growth rate for modes with no spanwise variation, in which case it corresponds to vortex pairing. The calculated and observed growth rates of the pairing instability are in good agreement. Pairing can also take place, albeit at reduced growth rates, in a three-dimensional form which would lead to a branched vortex structure similar to that which has been observed in the later stages of shear-layer development. Shear-layer growth by vortex amalgamation and generation of three-dimensionality by localized pairing are thus associated with the subharmonic instabilities. The translative instability, on the other hand, may be associated with the streamwise streak structure, and represents a distinct mechanism for the generation of three-dimensional motions.

A striking feature of the translative instability is its broadband nature, and in particular its high growth rate at short spanwise wavelengths. This characteristic suggests that, once the relatively smooth two-dimensional vortex structure has developed, energy can be transferred directly to small three-dimensional scales of a size limited only by dissipation, via the translative instability. This is rather different from the usual picture of stepwise turbulent cascade. In addition, the broad growth rate maximum implies that many spatial scales can be introduced simultaneously; such a richness of scales is decidedly characteristic of turbulence. We note that Orszag & Patera (1980) have discovered a similar broadband instability in their study of subcritical transition in plane channel flows. This suggests that instabilities leading to a direct cascade to small scales may be a general feature of the two-dimensional non-parallel flow instability problem.

Much additional work remains to be done in order to complete the characterization of the instabilities of coherent shear-layer vortices. For example, we have centred attention only on the fundamental mode ($\alpha = 0$) and first subharmonic mode ($\alpha = 1$) instabilities, even though α is a continuous parameter of the stability problem. Although we have ascertained that the first subharmonic mode is very nearly the most unstable mode with regard to two-dimensional instabilities, the parametric dependence of the three-dimensional instabilities on α has not yet been explored. Similarly, additional vorticity distributions and small core sizes need to be studied, in order to cover a wider range of experimentally realizable situations. Finally, the effect of nonlinearity on the development of the instabilities – and in particular on the competition between the two- and three-dimensional modes – needs to be investigated. Because of the complexity of the flow, there is little hope for progress on this latter problem outside of a full three-dimensional numerical simulation.

There is a lack of quantitative data on the rate of growth of controlled three-dimensional disturbances, which has somewhat limited numerical comparisons of our calculated growth rates with observations. It is suggested that a vibrating ribbon experiment in which the spanwise wavenumber and the frequency of the vibration can be varied independently would be informative. With such an apparatus, subharmonic and fundamental mode disturbances of definite spanwise scale could be excited, and their growth monitored downstream with a rake of hot-wire anemometers. The broadband nature of the instabilities, however, may make detailed comparison between theory and experiment difficult.

The computational work reported herein was made possible by the generous provision of computer time by the NOAA Geophysical Fluid Dynamics Laboratory,

Princeton, N.J. We are also grateful for the financial support provided to R.T.P. while in residence at the GFDL during the summer months of 1979. We have had the benefit of a number of informative conversations with Dr I. Orlanski of the GFDL.

This work was supported in part by the National Science Foundation under Contracts 7414978-ENG and 79-16877-CME, and by the Air Force Office of Scientific Research under Contract 79-0006.

REFERENCES

BENNEY, D. J. & LIN, C. C. 1960 On the secondary motion induced by oscillations in shear flow. *Phys. Fluids* **3**, 656.

BERNAL, L. P., BREIDENTHAL, R. E., BROWN, G. L., KONRAD, J. H. & ROSHKO, A. 1979 On the development of three dimensional small scales in turbulent mixing layers. In *Proc. 2nd Int. Symp. on Turbulent Shear Flows, Imperial College, London.*

BLISS, D. B. 1973 Ph.D. dissertation, Massachusetts Institute of Technology.

BOYD, J. 1978 Spectral and pseudospectral methods for eigenvalue and nonseparable boundary value problems. *Monthly Weather Rev.* **106**, 1192–1203.

BREIDENTHAL, R. E. 1978 A chemically reacting turbulent shear layer. Ph.D. thesis, California Institute of Technology.

BROWAND, F. K. & TROUTT, T. 1980 A note on spanwise structure in the two-dimensional mixing layer. *J. Fluid Mech.* **97**, 771.

BROWAND, F. K. & WEIDMAN, P. D. 1976 Large scales in the developing mixing layer. *J. Fluid Mech.* **76**, 127.

BROWN, G. L. & ROSHKO, A. 1974 On density effects and large structures in turbulent mixing layers. *J. Fluid Mech.* **64**, 775.

CHANDRSUDA, C., MEHTA, R. D., WEIR, A. D. & BRADSHAW, P. 1978 Effect of free-stream turbulence on large structure in turbulent mixing layers. *J. Fluid Mech.* **85**, 693.

GOTTLIEB, D. & ORSZAG, S. A. 1977 *Numerical Analysis of Spectral Methods: Theory and Applications*, S.I.A.M. Regional Conf. Series in Appl. Math., vol. 26.

KELLY, R. E. 1967 On the stability of an inviscid shear layer which is periodic in space and time. *J. Fluid Mech.* **27**, 657.

LAMB, H. 1932 *Hydrodynamics*, 6th edn, pp. 156, 224. Dover.

MANSOUR, N. N., FERZIGER, J. & REYNOLDS, W. C. 1978 Large eddy simulation of a turbulent mixing layer. *Thermosci. Rep.* TF-11 *Div., Dept. of Mech. Engng, Stanford Univ.*

MIKSAD, R. W. 1972 Experiments on the nonlinear stages of free shear layer transition. *J. Fluid Mech.* **56**, 645.

MOORE, D. W. & SAFFMAN, P. G. 1975*a* The density of organized vortices in a turbulent mixing layer. *J. Fluid Mech.* **69**, 465.

MOORE, D. W. & SAFFMAN, P. G. 1975*b* The instability of a straight vortex filament in a strain field. *Proc. R. Soc. Lond.* A **346**, 413.

ORSZAG, S. A. & PATERA, A. 1980 Subcritical transitions to turbulence in plane channel flows. *Phys. Rev. Lett.* **45**, 989.

PIERREHUMBERT, R. T. & WIDNALL, S. E. 1981 The structure of organized vortices in a free shear layer. *J. Fluid Mech.* **102**, 301.

ROSHKO, A. 1976 *Structure of Turbulent Shear Flows: A New Look. A.I.A.A. J.* **14**, 1349.

SMITH, B. T., BOYLE, J. M., DONGARRON, J. J., GARBOW, B. S., IKEBE, Y., KLEMA, V. C. & MOLER, C. B. 1974 *Matrix Eigensystem Routines–EISPACK Guide*, Lecture Notes in Computer Science, vol. 6. Springer.

STUART, J. T. 1967 On finite amplitude oscillations in laminar mixing layers. *J. Fluid Mech.* **29**, 417.

TSAI, C. Y. & WIDNALL, S. E. 1976 The stability of short waves on a straight vortex filament in a weak externally imposed strain field. *J. Fluid Mech.* **73**, 721.

WINANT, C. D. & BROWAND, F. K. 1974 Vortex pairing: the mechanism of turbulent mixing-layer growth at moderate Reynolds number. *J. Fluid Mech.* **63**, 237.

WYGNANSKI, I., OSTER, D., FIEDLER, H. & DZIOMBA, B. 1979 On the perseverance of a quasi-two-dimensional eddy-structure in a turbulent mixing layer. *J. Fluid Mech.* **93**, 325.